Research Square

Preprints are preliminary reports that have not undergone peer review.
They should not be considered conclusive, used to inform clinical practice,
or referenced by the media as validated information.

Microwave-Assisted Catalytic Pyrolysis of Polypropylene Waste Plastics for Hydrogen-Rich Gas Production with Ni-Fe/γ- Al_2O_3 Catalyst

Limin Hou
Inner Mongolia University of Science and Technology
Yabin Wang
Inner Mongolia University of Science and Technology
Yerong Shi
Inner Mongolia University of Science and Technology
Yuxuan Sui
Inner Mongolia University of Science and Technology
Dedan Duan
183068470950163.com

Inner Mongolia University of Science and Technology
Zhiyu Zhang
Inner Mongolia University of Science and Technology

Research Article

Keywords: Polypropylene, Ni-Fe catalyst, Microwave pyrolysis, Activated carbon absorber, Hydrogen-rich gas

Posted Date: November 16th, 2026

DOI: https://doi.org/10.21203/rs.3.rs-11448869/v1

License: This work is licensed under a Creative Commons Attribution 4.0 International License.
Read Full License

Additional Declarations: No competing interests reported.

Microwave-Assisted Catalytic Pyrolysis of Polypropylene Waste Plastics for Hydrogen-Rich Gas Production with Ni-Fe/γ-Al_2O_3 Catalyst

Limin Hou [a b], Yabin Wang [a], Yerong Shi [a], Yuxuan Sui [a], Dedan Duan [a], Zhiyu Zhang [a b]*

[a] *School of Energy and Environment, Inner Mongolia University of Science and Technology, Baotou 014010, China*

[b] *School of Energy Industry, Inner Mongolia University of Science and Technology, Baotou 014010, China*

**Corresponding author. E-mail: 18306847095@163.com*

Limin Hou: neuhlm@163.com

Yabin Wang: 3243721096@qq.com

Yerong Shi: 3406588483@qq.com

Yuxuan Sui: 1084458435@qq.com

Dedan Duan: 18306847095@163.com

Zhiyu Zhang; zzy0021@126.com

Abstract: Global plastic waste continues to increase, while conventional disposal methods such as landfilling and incineration both waste resources and pollute the environment. Converting polypropylene (PP) into hydrogen offers a potential route toward low-carbon hydrogen production with environmental benefits. This study used polypropylene (PP) as the feedstock and prepared the Ni-Fe/γ-Al_2O_3 bimetallic catalyst by impregnation, with activated carbon as the microwave absorber. The effects of absorber type (coconut-shell, wood-based, and coal-based), catalyst-to-absorber mass ratio (5:2, 5:3, 5:4, and 1:1), and microwave power (1200 to 1800 W) on hydrogen production were systematically examined, and XRD, SEM, and FT-IR were used to follow the phase evolution of the catalyst. Coconut-shell activated carbon offered favorable energy conditions for PP pyrolysis, as its well-developed microporous structure enabled efficient microwave absorption. Its self-gasification also partially contributed to gas production. Under the optimal conditions of 5:4 catalyst-to-absorber mass ratio and 1600 W microwave power, H_2 yield reached 77.1 mmol/g_{pp}, H_2 efficiency 88.6%, and H_2 composition 80.1 vol.%, whereas CO, CO_2, CH_4, and C_2-C_5 were formed only as minor by-products. This study explored the synergistic behavior of the activated carbon absorber and the

Ni-Fe catalyst in the microwave field, providing experimental data and process guidance for the valorization of waste plastics into hydrogen-rich gas.
Keywords: Polypropylene; Ni-Fe catalyst; Microwave pyrolysis; Activated carbon absorber; Hydrogen-rich gas

1 Introduction

Since the 1950s, plastics have been mass-produced and widely used because of their light weight, durability, and low cost. Of the 49 billion tonnes produced to date, only approximately 9% have been recycled, 12% incinerated, and 79% landfilled or discarded in the natural environment [1], and plastic pollution has become a global environmental crisis. Meanwhile, hydrogen, with a chemical energy density of 120 MJ/kg, is a key candidate for future clean energy. However, approximately 96% of global hydrogen production currently relies on fossil-fuel reforming, and this process emits about 830 million tonnes of CO_2 annually [2]. With a hydrogen content of 8-14 wt% [3], plastics are a promising feedstock for hydrogen production from plastic pyrolysis. Plastic pyrolysis for hydrogen can both reduce waste and produce clean energy, opening up new research directions connecting plastic waste treatment with hydrogen production.

Compared with conventional conductive heating, microwave pyrolysis heats materials directly from within through dipole rotation (dipolar polarization), interfacial polarization, and ionic motion [4]. This provides rapid, uniform, and selective heating along with high efficiency and short processing times [5]. Irfan et al. [6] demonstrated that microwave irradiation can promote plastic pyrolysis to produce high-purity H_2 and carbon nanotubes, indicating clear potential for resource conversion. Microwave pyrolysis performance depends on several factors. With respect to temperature, pyrolysis oil is the dominant product in the 300-500 °C range, whereas the proportion of gaseous products rises sharply above 500 °C [7]. Gas yield also varies with plastic type, following the order PP > PE > PS because of differences in molecular chain structure: the methyl side chain of PP weakens C-C bonds, making it more susceptible to β-scission [8]. For microwave power, Suriapparao et al. [9] found that increasing power shortens pyrolysis time and promotes secondary reactions that generate more volatile products. Among catalyst systems, zeolite molecular sieves and metal-supported catalysts are commonly used [10]. Metal-supported catalysts, especially Ni-Fe bimetallic catalysts, can enhance H_2 selectivity and yield through synergistic effects. Yao et al. [11] applied the Ni-Fe catalyst to plastic pyrolysis and obtained a fourfold increase in hydrogen production efficiency compared with that of the control group. Luo et al. [12] developed the Fe-Ni/SiC catalyst with SiC as the support, achieving 73.89% H_2 selectivity in microwave-assisted catalytic pyrolysis of LDPE, 60% higher than that of monometallic catalysts. Ni-based catalysts are widely used because they are highly active in C-H bond activation and dehydrogenation, but their thermal stability and resistance to carbon deposition are limited. Fe-based catalysts have redox properties that promote carbon chain cracking and the removal of carbon deposits [13]. Plastics

themselves absorb microwaves very poorly, so absorbers are essential to the system. Carbonaceous absorbers such as activated carbon may also participate chemically in pyrolysis through self-gasification and contribute to gaseous products. The choice and dosage of absorber strongly affect pyrolysis efficiency. Liu et al. [14] prepared the Ni-Fe-coated catalyst using porous SiC foam as the microwave absorber for hydrogen production. The sample reached 450 °C in just 260 s under 400 W microwave irradiation, whereas the conventional physical mixing system needed 800 W to achieve the same heating rate. However, SiC has poor mechanical strength, which can cause surface agglomeration and loss of active components, reducing catalytic stability. In contrast, Al_2O_3, with its tunable pore structure, large specific surface area, acidic surface, and excellent thermal stability, has become the preferred support for catalytic pyrolysis of plastics into hydrogen [15].

In this study, PP was the feedstock, paired with the Ni-Fe/γ-Al_2O_3 catalyst and an activated carbon absorber. The effects of absorber type, catalyst-to-absorber mass ratio, and microwave power on product distribution and hydrogen production performance were investigated. XRD, SEM, and FT-IR were used to characterize the catalyst before and after the reaction and to investigate the synergy between the activated-carbon absorber and the Ni-Fe catalyst.

2 Experimental

2.1 Materials and Instruments

The feedstock used was polypropylene (PP) particles (100 mesh, 99.9% purity), supplied by Jinheng Plastic Co., Ltd. Three types of powdered activated carbon-coconut-shell, wood-based, and coal-based (all 200 mesh)—were purchased from Wuxi Xingzhiguang Activated Carbon Co., Ltd. and used as microwave absorbers. Table 1 presents the elemental composition of the three activated carbons; Table 2 and Table 3 list the chemical reagents and instruments used in this experiment, respectively.

Table 1 Elemental analysis of activated carbon

Activated carbon type	C/%	H/%	O/%	N/%	S/%
Coconut-shell AC	68.563	4.172	27.052	0.193	0.02
Wood-based AC	71.623	2.657	25.374	0.282	0.064
Coal-based AC	71.716	1.389	25.135	0.242	1.518

Table 2 Chemical reagents

Name	Chemical formula	Purity/Specification	Manufacturer
Ferric nitrate nonahydrate	$Fe(NO_3)_3 \cdot 9H_2O$	Analytical grade	Macklin Biochemical Co.,Ltd
Nickel acetate tetra hydrate	$Ni(CH_3COO)_2 \cdot 4H_2O$	Analytical grade	Macklin Biochemical Co.,Ltd
Activated alumina	γ-Al_2O_3	Analytical grade	Macklin Biochemical Co.,Ltd
Absolute ethanol	C_2H_5OH	99.99%	Macklin Biochemical Co.,Ltd

Table 3 Instruments and equipment

Instrument	Model	Manufacturer
Magnetic stirrer	HJ-6B	Xicheng Xinrui Instrument Factory,Jintan District, Jiangsu, China
Electric blast drying oven	Type 101	Yongguangming Medical Instrument Factory, Beijing, China
Muffle furnace	HMF 1200-30/30/40	Shanghai Haoyue Vacuum Equipment Co.,Ltd.

2.2 Preparation of Ni-Fe/γ-Al_2O_3 Catalyst

The Ni-Fe/γ-Al_2O_3 catalyst was prepared by the impregnation method, comprising four main steps: reagent weighing, constant-temperature magnetic stirring, oven drying, and muffle furnace calcination. The specific procedure was as follows: 10.86 g of ferric nitrate nonahydrate ($Fe(NO_3)_3 \cdot 9H_2O$), 4.46 g of nickel acetate tetrahydrate ($Ni(CH_3COO)_2 \cdot 4H_2O$), and 3.5 g of activated alumina (γ-Al_2O_3) were dissolved in 25 mL of anhydrous ethanol. The mixed solution was magnetically stirred at 60°C for 6 h, followed by drying in an oven at 110°C for 12 h. The dried sample was then ground, passed through a 100-mesh sieve, and calcined in a muffle furnace at the desired temperature for 2 h. After natural cooling for 18 h, the Ni-Fe/γ-Al_2O_3 catalyst was obtained.

2.3 Experimental Procedure

Figure 1 shows schematic of the microwave-assisted catalytic pyrolysis system. It mainly consisted of a gas supply system, a microwave thermogravimetric reactor, a condenser system, and a gas analysis system. The microwave output power of the microwave thermogravimetric reactor was continuously adjustable within the range of 0.2-2.00 kW, with an output frequency of 2.45 GHz ± 25 MHz. During the reaction, the surface temperature of the crucible was

measured in real time by the thermocouple integrated into the analyzer. Because microwaves penetrate and heat materials from within, the interior of the material was typically hotter than its surface during pyrolysis [16]. The thermocouple reading therefore approximated the bulk temperature of the material. Temperature (T) versus time (t) curves were recorded during the microwave experiments.

PP was physically mixed with the catalyst at a mass ratio of 1:1 (0.5 g of PP per experiment). Activated carbon absorbers of different types and proportions were then placed on top of the mixture. The sample was loaded into a quartz crucible (33 mm in diameter), which was then placed at the axial center of the microwave heating chamber. Before pyrolysis, N_2 was introduced at 100 mL/min for 10 min to purge the system, ensuring a nitrogen-protected atmosphere. During the reaction, liquid products were collected by condensation in a cold trap, and non-condensable gases were collected in gas sampling bags. After the reaction, N_2 was introduced at 80 mL/min for 45 min to sweep residual gases into sampling bags. The total gas volume was measured, and the composition was determined with the gas analyzer. To ensure data reliability and reproducibility, each experiment was repeated at least three times, and average values were reported.

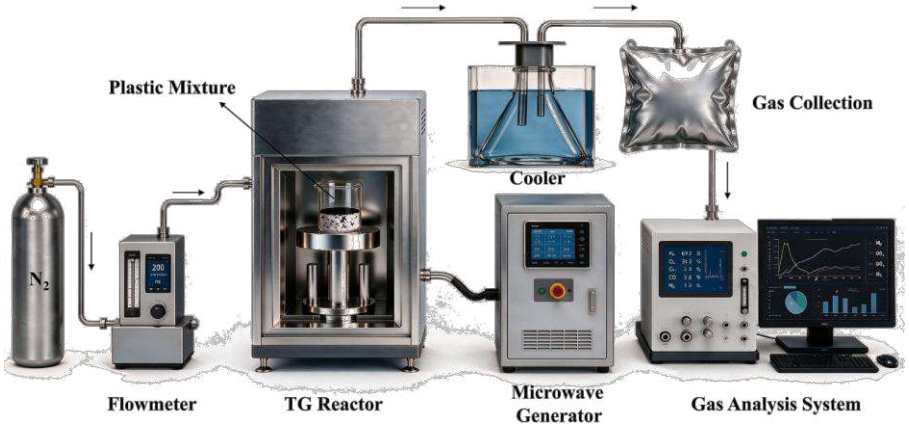


Figure 1 Microwave-assisted plastic pyrolysis hydrogen production reaction system

2.4 Experimental Data Processing

The volume percentage of product composition obtained from the gas analyzer is defined as selectivity, and the mass of each gaseous product is calculated based on the gas volume and composition measured by the gas analyzer. Therefore, the H_2 yield was defined as the molar amount of H_2 divided by the total mass of plastic (PP) and activated carbon (Eq. 1). The H_2 efficiency was determined by dividing the total mass of hydrogen contained in all gaseous products by the theoretical mass of hydrogen in the plastic (Eq. 2). The gas yield was determined by dividing the mass of gas obtained by the total mass of plastic and activated

carbon (Eq. 3). The solid (carbon) yield was determined by dividing the mass difference of the sample before and after the reaction by the total mass of plastic and activated carbon (Eq. 4). The volatile (liquid) products during the reaction were determined by dividing the mass difference of the flask before and after reaction by the total mass of plastic and activated carbon (Eq. 5).

$$H_2\ \text{Yield} = \frac{\text{Moles of Generated } H_2\,(\text{mmol})}{\text{Mass of Plastic and Activated Carbon(g)}}\,(\text{mmol}\cdot g_{PP}^{-1}) \tag{1}$$

$$H_2\ \text{Efficiency} = \frac{\text{Total Mass of H in All Gaseous products(g)}}{\text{Theoretical Mass of H in Plastic(g)}}\,(\%) \tag{2}$$

$$\text{Solid Yield} = \frac{\text{Weight Difference of Solid Before and After Reaction(g)}}{\text{Mass of Plastic and Activated Carbon(g)}} \times 100\%(\text{wt\%}) \tag{3}$$

$$\text{Gas Yield} = \frac{\text{Mass of Gas(g)}}{\text{Mass of Plastic and Activated Carbon(g)}} \times 100\%(\text{wt\%}) \tag{4}$$

$$\text{Liquid Yield} = \frac{\text{Mass Difference of the Flask Before and After Reaction}}{\text{Mass of Plastic and Activated Carbon}} \times 100\%(\text{wt\%}) \tag{5}$$

2.5 Characterization Methods

X-ray diffraction (XRD) analysis was performed using the PANalytical X'pert3 X-ray diffractometer (Netherlands) with Cu Kα radiation (λ = 1.5406 Å). The tube voltage and current were 40 kV and 40 mA, respectively, with a scanning range of 10°-80° at 5 °/min. Phase composition and crystal structure were determined from the positions and relative intensities of the diffraction peaks. Scanning electron microscopy (SEM) analysis was performed using the COXEM EM-30 field-emission scanning electron microscope, which exploits electron-sample interactions to characterize surface morphology via secondary electron imaging. The magnification was adjustable from 200× to 500,000×. Images in this experiment were recorded at 10,000× to show catalyst particle size, morphology, and surface pore distribution. Fourier-transform infrared (FT-IR) spectroscopy was performed using the Nicolet 380 spectrometer, with a spectral range of 4000-400 cm^{-1} and a resolution of 4 cm^{-1}. Surface chemical bonds and molecular structures were identified from characteristic absorption peaks.

3 Results and discussion

3.1 Effect of Absorber Type on Hydrogen Production Performance of PP Microwave Pyrolysis

3.1.1 Heating Characteristics

Figure 2 shows the heating curves of microwave pyrolysis of PP with different activated carbon absorbers. With no absorber added, the mixed sample underwent an initial slow heating

stage with a heating rate of only 51 °C/min. After adding coconut-shell, wood-based, and coal-based activated carbon, the heating rates rose to 60, 82, and 74 °C/min, respectively, and all samples exceeded 450 °C quickly. This shows that activated carbon absorbs microwave energy effectively and conducts heat uniformly, creating the temperature conditions needed for bond cleavage and catalytic dehydrogenation in the plastic. The three activated carbons differed in their heating characteristics. Wood-based activated carbon heated most rapidly, but its loose macroporous structure allowed too little contact time between plastic particles and the catalyst active sites, so many intermediates escaped as liquid before deep dehydrogenation could occur. Coconut-shell activated carbon heated steadily, absorbing and releasing microwave energy uniformly. This avoided local overheating and gave more time for plastic to contact the catalyst and for C-C and C-H bond cleavage, which increased gas yield and H_2 selectivity. These results confirm that the type of activated carbon affects both the heating rate and temperature field stability through its microwave absorption and energy conversion efficiency.

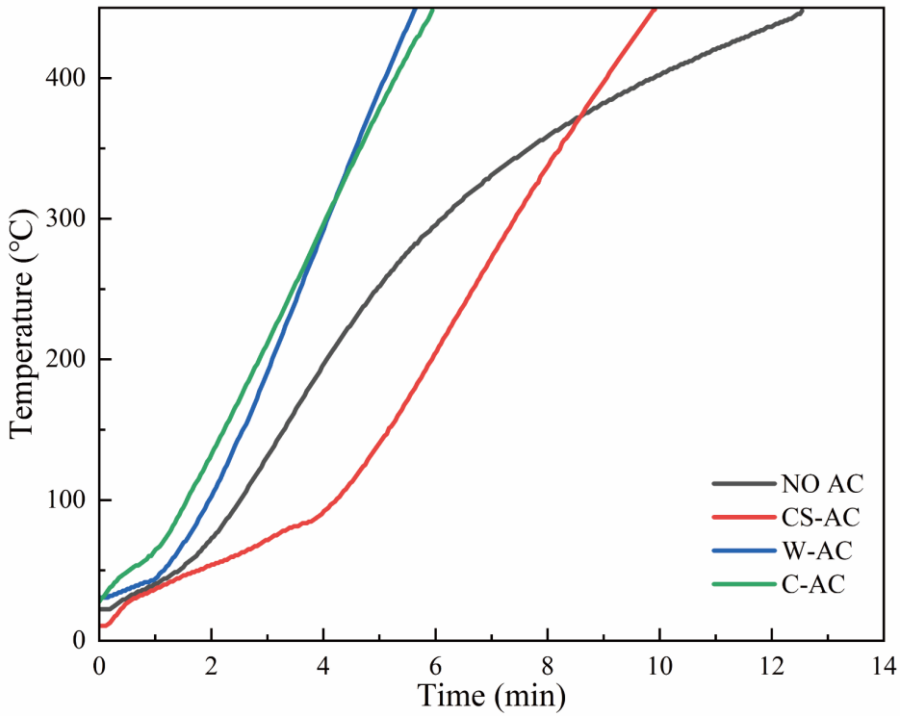


Figure 2 Heating curves of microwave pyrolysis of PP with different types of activated carbon absorbers

3.1.2 Product Distribution and Hydrogen Production Performance

Figure 3 shows the hydrogen production performance of microwave pyrolysis of PP with different activated carbon absorbers. With no absorber added, PP particles alone absorbed microwaves very poorly, and the temperature did not reach the threshold for significant PP pyrolysis, so little pyrolysis occurred. The H_2 yield was only 1.4 mmol/g_{pp}, and H_2 efficiency

was nearly 0%. With activated carbon added, hydrogen production improved substantially. The coconut-shell, wood-based, and coal-based systems gave H_2 yields of 77.1, 63.6, and 58.2 mmol/g_{pp}, and H_2 efficiencies of 88.6%, 78.5%, and 76.6%, respectively. Without activated carbon added, the theoretical H_2 yield was 70.5 mmol/g_{pp}. Upon addition of coconut-shell, wood-based, and coal-based activated carbons, the theoretical H_2 yields were 87.1, 81.0, 76.0 mmol/g_{pp}, respectively. This can be attributed to their different hydrogen contents (Table 1), which are 4.2, 2.7 and 1.4 wt.%, respectively. The coconut-shell system achieved the highest H_2 yield and efficiency, showing that coconut-shell activated carbon and the Ni-Fe catalyst had the strongest synergistic effect on hydrogen production. It should be noted that the self-gasification of activated carbon also contributed to hydrogen production.

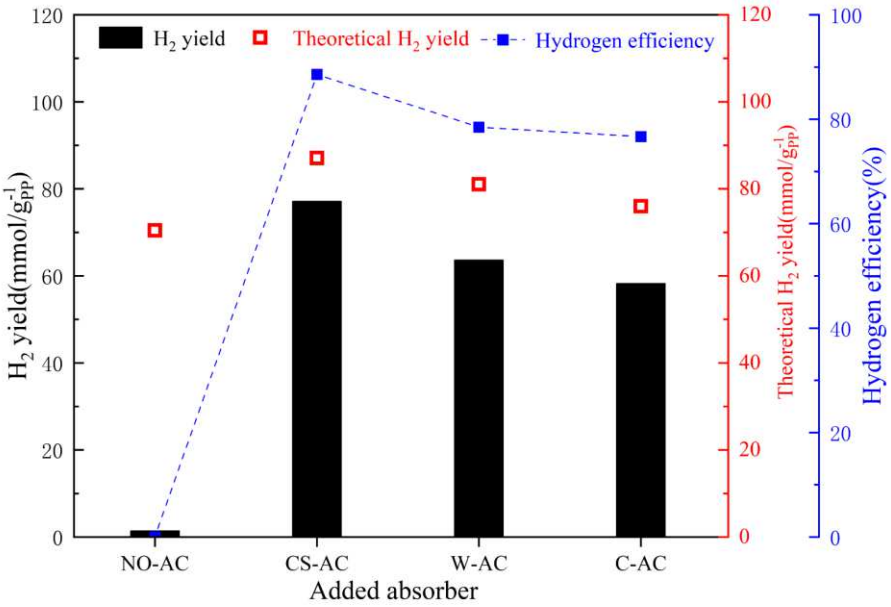


Figure 3 H_2 yield, theoretical yield, and hydrogen production efficiency after microwave pyrolysis of PP with different types of activated carbon absorbers. NO AC = no activated carbon; CS-AC = coconut-shell activated carbon; W-AC = wood-based activated carbon; C-AC = coal-based activated carbon

Figure 4 shows the product distribution and gas composition of microwave pyrolysis of PP with different activated carbon absorbers. With no absorber added, the H_2 composition was only 34.5 vol.%, the gas yield only 9.2 wt.%, the solid residue 84.9 wt.%, and the liquid yield 5.9 wt.%; CO and CO_2 accounted for 44.2 and 21.4 vol.%, respectively. With activated carbon added, the H_2 compositions were 80.1, 77.2, and 77.2 vol.%, respectively. The coconut-shell system gave 39.0 wt.% gas, 51.4 wt.% solid, and 9.5 wt.% liquid; the wood-based system gave 36.6, 49.2, and 14.1 wt.%; and the coal-based system gave 35.6, 51.9, and 13.4 wt.%. As for the gas composition, all three systems were dominated by H_2 and CO. In the coconut-shell

system, H_2 accounted for 80.1 vol.%, CO for 15.9 vol.%, CO_2 for 1.1 vol.%, CH_4 for 1.8 vol.%, and C_2-C_5 for 1.1 vol.%. The wood-based and coal-based systems had higher proportions of CO, CH_4, and C_2-C_5, showing that deep cracking and reforming were less complete than in the coconut-shell system. The product gas heating value peaked at 11.1 MJ/m³ for the coconut-shell activated carbon system.

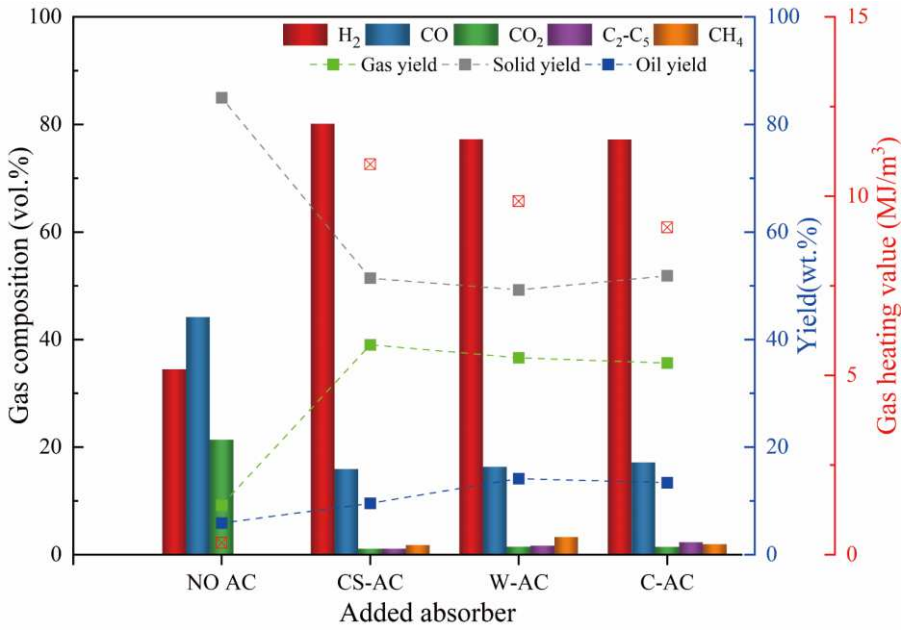


Figure 4 Product distribution and gas composition after microwave pyrolysis of PP with different types of activated carbon absorbers

3.1.3 Phase Composition Analysis

Figure 5 shows the phase composition of solid products before and after microwave pyrolysis of PP with different activated carbons. XRD patterns show that before the reaction, the catalyst was present as $NiFe_2O_4$ spinel and γ-Al_2O_3. After the reaction, these peaks largely disappeared and were replaced by Fe_3C, Fe_3O_4, and $Ni_{0.36}Fe_{0.64}$ solid solution phases. The characteristic diffraction peaks of PP disappeared completely, indicating that crystalline PP was fully converted; some PP-derived carbon may have remained as amorphous carbon or as low-molecular-weight organic matter. This confirms that the active components of the catalyst were reduced in situ during pyrolysis and participated in the complete conversion of PP. Consistent with the product distribution and hydrogen production results, the diffraction peak intensities of Fe_3C, Fe_3O_4, and $Ni_{0.36}Fe_{0.64}$ were highest in the coconut-shell system, whereas in the wood-based and coal-based systems the active-phase peaks were weaker and the broad amorphous-carbon peak was enhanced. According to literature reports, Fe_3C is a key active intermediate for catalytic dehydrogenation, inducing thermal cleavage of C-C bonds [17].

$Ni_{0.36}Fe_{0.64}$ and Fe_3O_4 are regarded as the active phases of the catalyst, with Fe_3O_4 sites preferentially catalyzing C-H bond cleavage [18]. Higher diffraction peak intensities of Fe_3C, Fe_3O_4, and $Ni_{0.36}Fe_{0.64}$ indicate higher relative contents of the corresponding crystalline phases and thus a larger number of active sites.

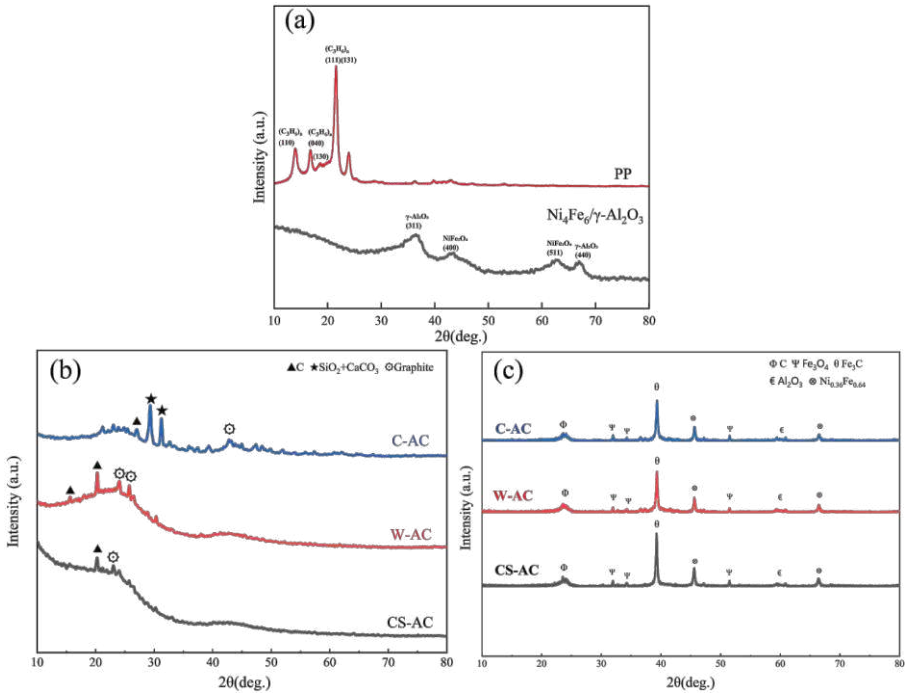


Figure 5 Phase composition of pre-reaction solids and post-reaction solid products from microwave pyrolysis of PP with different types of activated carbons

(a) 100-mesh PP particles and Ni-Fe/γ-Al_2O_3 catalyst; (b) activated carbon absorber; (c) products after microwave pyrolysis of PP with different types of activated carbon

3.1.4 Functional Group Analysis

Figure 6 shows the functional groups and molecular structures of solid products before and after microwave pyrolysis of PP with different activated carbons. Before the reaction, PP showed characteristic absorption peaks at 2910, 1460, and 1059 cm^{-1}, corresponding to stretching vibrations of $-CH_3$ and $-CH_2-$. After catalytic pyrolysis, all PP characteristic peaks disappeared, with only a very weak absorption peak of $-CH_3$ remaining, indicating that the PP macromolecular chains were largely broken down. Among the three systems, the coconut-shell solid product had the weakest peak at 400-700 cm^{-1}, assigned to the long-chain aliphatic C-C skeleton, suggesting less residual disordered carbon and more thorough PP pyrolysis. The coal-based system had the strongest peak, indicating that its lower specific surface area and uneven heat distribution led to insufficient PP pyrolysis, with more long-chain aliphatic carbon skeletons retained in the solid product.

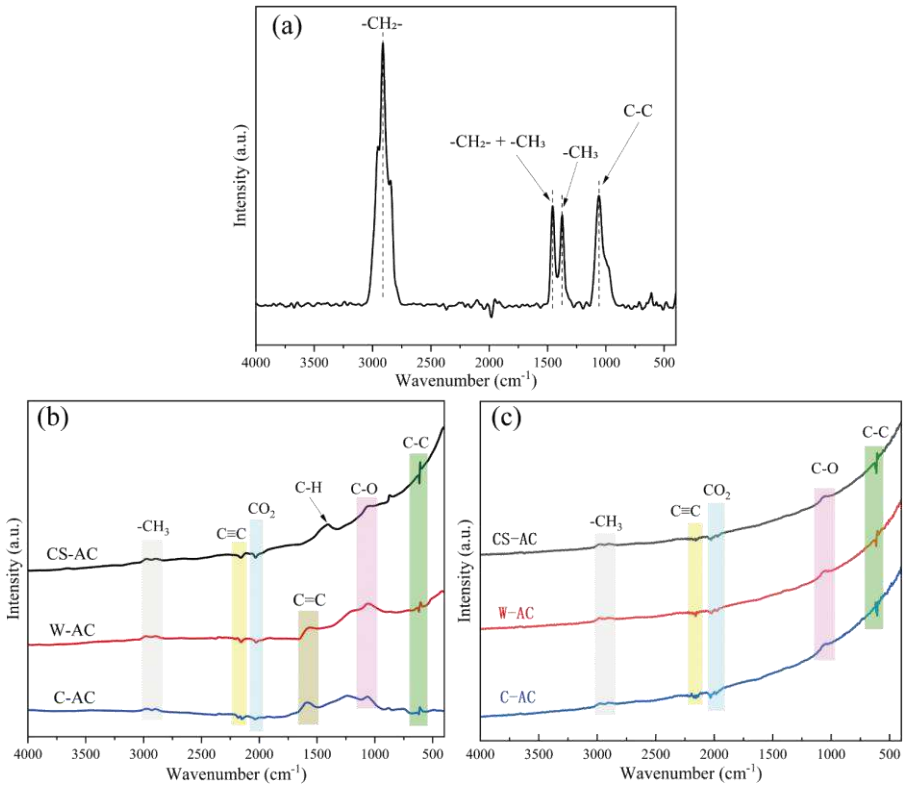


Figure 6 Functional groups and molecular structures of pre-reaction solids and post-reaction solid products from microwave pyrolysis of PP with different types of activated carbons (a) Plastic particles; (b) activated carbon absorber; (c) solid products after microwave pyrolysis of PP with different activated carbon absorbers

3.1.5 Morphology Analysis

Figure 7 shows the surface morphology of solid products after microwave pyrolysis of PP with different activated carbons. The product with coconut-shell activated carbon was loose, finely fragmented, and uniformly distributed, which can be attributed to its high specific surface area and abundant microporous structure. These structural features promoted efficient microwave absorption and conversion, thereby facilitating deep pyrolysis and dehydrogenation of PP. In contrast, the products with wood-based and coal-based activated carbon showed extensive agglomeration and pronounced sintering. This was because both carbons had lower specific surface areas and microporosities, less uniform pore-size distributions, and higher impurity contents, which caused uneven heat distribution in the catalyst and excessively rapid local heating. This led to sintering of incompletely pyrolyzed plastic macromolecules and encapsulation of some active sites by carbon, reducing catalytic capacity.

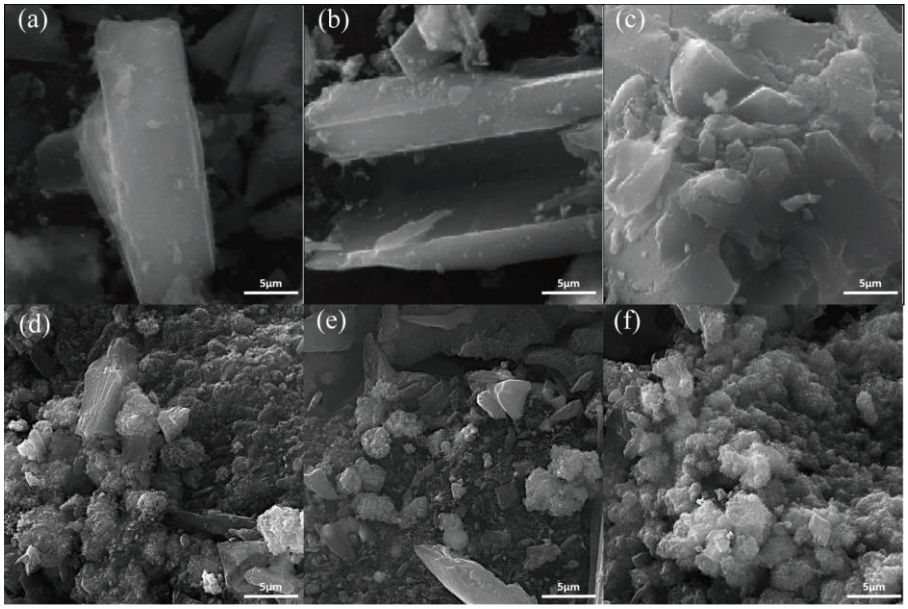


Figure 7 Microstructure of pre-reaction solids and post-reaction solid products from microwave pyrolysis of PP with different types of activated carbons

(a), (b), (c) Coconut-shell, wood-based, and coal-based activated carbon; (d), (e), (f) products after microwave pyrolysis of PP with different activated carbon absorbers

3.1.6 Specific Surface Area and Pore Structure Analysis

Table 4 shows that coconut-shell activated carbon had much higher specific surface area (1676.14 m^2/g) and micropore volume (1.50 mL/g) than wood-based (1093.57 m^2/g, 1.01 mL/g) or coal-based activated carbon (688.11 m^2/g, 0.82 mL/g). Its well-developed microporous structure absorbs microwaves efficiently and converts them to uniform heat, avoiding local hotspots. It also extends the residence time of volatiles on catalyst active sites, promoting deep dehydrogenation and secondary cracking of intermediates and increasing H_2 yield and selectivity. Thus, the specific surface area and pore structure of activated carbon govern its microwave absorption and catalytic synergy. Of the three, coconut-shell activated carbon, with the highest specific surface area and a micropore-dominated structure, gave the best hydrogen production performance in microwave-assisted catalytic pyrolysis.

Table 4 Specific surface area, pore volume, and pore size of activated carbon

Activated carbon type	Specific surface area (m^2/g)	Pore volume (mL/g)	Average pore size (nm)
Coconut-shell AC	1676.14	1.50	3.58
Wood-based AC	1093.57	1.01	3.72

Coal-based AC	688.11	0.82	4.76

3.2 Effect of Catalyst-to-Absorber Mass Ratio on Hydrogen Production Performance

3.2.1 Heating Characteristics

Figure 8 shows the heating curves of microwave pyrolysis of PP at different catalyst-to-absorber mass ratios. At ratios of 5:2, 5:3, 5:4, and 1:1, the average heating rates after 3 min were 74.5, 73.8, 67.9, and 90.4 °C/min, respectively. The heating curve for the 5:4 sample was the most gradual, showing that coconut-shell activated carbon at this ratio transferred absorbed microwave energy steadily and uniformly to the surrounding PP particles and catalyst, avoiding local overheating and uneven heating, and favoring thorough pyrolysis and dehydrogenation of macromolecular chains at the active sites. The 5:2 and 5:3 systems contained less absorber, so the mixed system absorbed microwaves poorly and converted them to heat less efficiently, leaving PP particles incompletely pyrolyzed. At 1:1, the system heated most rapidly, so volatile intermediates from PP pyrolysis spent too little time on the catalyst active sites, which reduced H_2 production and gas yield.

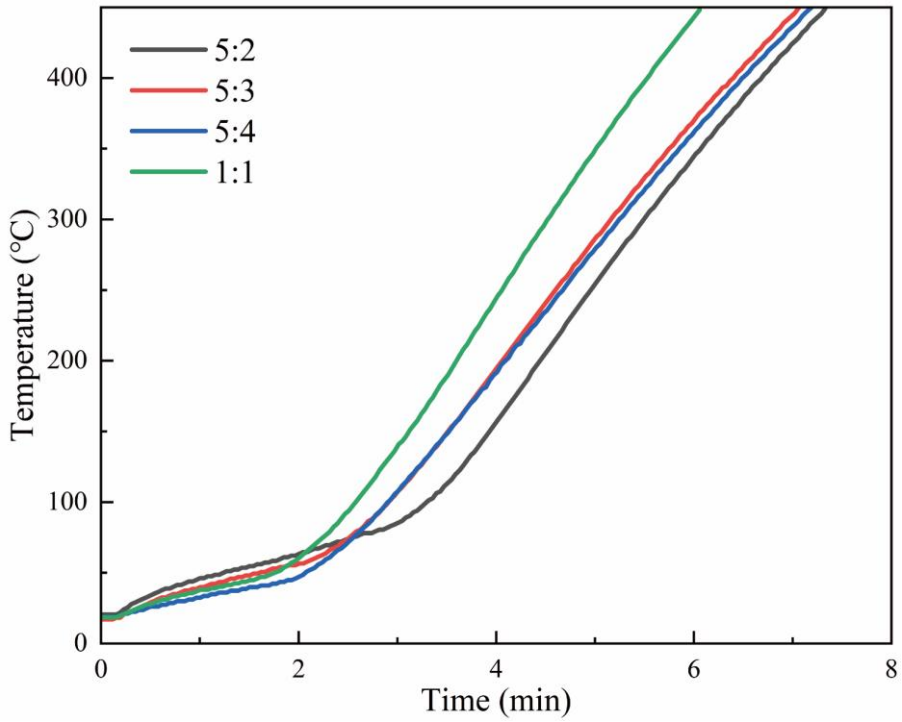


Figure 8 Heating curves of microwave pyrolysis of PP at different catalyst-to-absorber mass ratios

3.2.2 Product Distribution and Hydrogen Production Performance

Figure 9 shows the hydrogen production performance of microwave pyrolysis of PP at different catalyst-to-coconut-shell-activated-carbon mass ratios. As the absorber proportion

increased, both H_2 yield and H_2 efficiency first increased and then decreased. At 5:2, the H_2 yield was 60.8 mmol/g_{pp}, with H_2 efficiency of 77.2%. At 5:3, the H_2 yield was 65.9 mmol/g_{pp}, with H_2 efficiency of 79.5%. Performance peaked at 5:4, with H_2 yield of 77.1 mmol/g_{pp} and H_2 efficiency of 88.6%, indicating that absorber capacity and catalyst activity were best matched at this ratio. At 1:1, the H_2 yield decreased to 72.5 mmol/g_{pp}, H_2 efficiency to 79.4%. As the proportion of coconut-shell activated carbon increased, the theoretical H_2 yield increased from 78.6 to 91.2 mmol/g_{pp}.

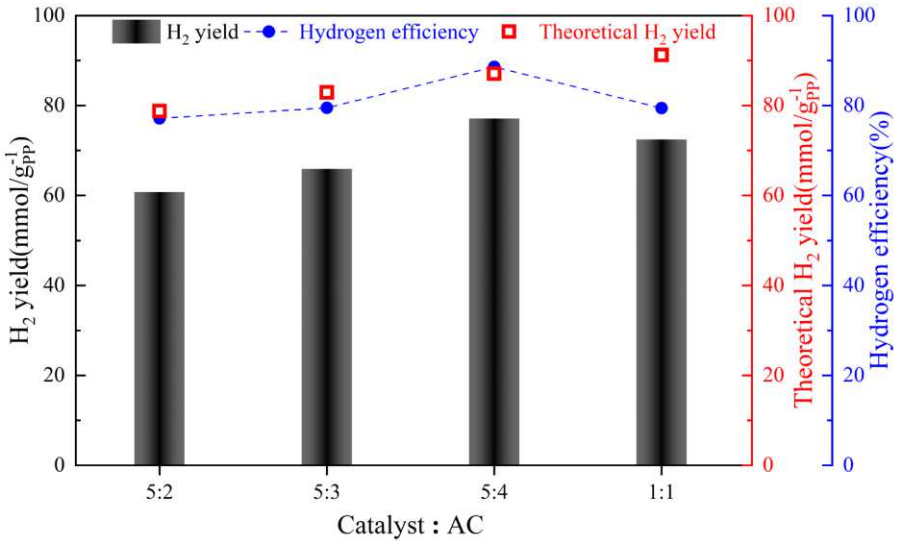


Figure 9 H_2 yield, theoretical yield, and hydrogen production efficiency after microwave pyrolysis of PP at different catalyst-to-absorber mass ratios

Figure 10 shows the product distribution and gas composition of microwave pyrolysis of PP at different catalyst-to-absorber mass ratios. Gas yield first increased and then decreased with rising absorber proportion, peaking at 5:4. From 5:2 to 5:4, gas yield increased from 38.6 to 39.0 wt.%, liquid yield decreased from 14.9 to 9.5 wt.%, solid yield increased from 44.6 to 51.4 wt.%, and the compositions of by-products such as CO_2, C_2-C_5, and CH_4 decreased. At 1:1, by contrast, gas yield decreased to 33.4 wt.%, liquid yield increased to 12.7 wt.%, and solid yield increased to 53.8 wt.%. As for the gas composition, the 5:4 system contained 80.1 vol.% H_2, 15.9 vol.% CO, 1.1 vol.% CO_2, 1.8 vol.% CH_4, and 1.1 vol.% C_2-C_5. In the 1:1 system, the H_2 composition decreased to 79.9 vol.%, whereas the CO composition increased to 16.6 vol.% and the CH_4 and C_2-C_5 fractions decreased slightly to 1.4 and 0.9 vol.%, respectively. This indicates that the excess absorber altered the reaction pathway, promoting CO formation but inhibiting hydrocarbon cracking. The product gas heating value first increased and then decreased with the increase of the mass ratio, peaking at 11.1 MJ/m^3.

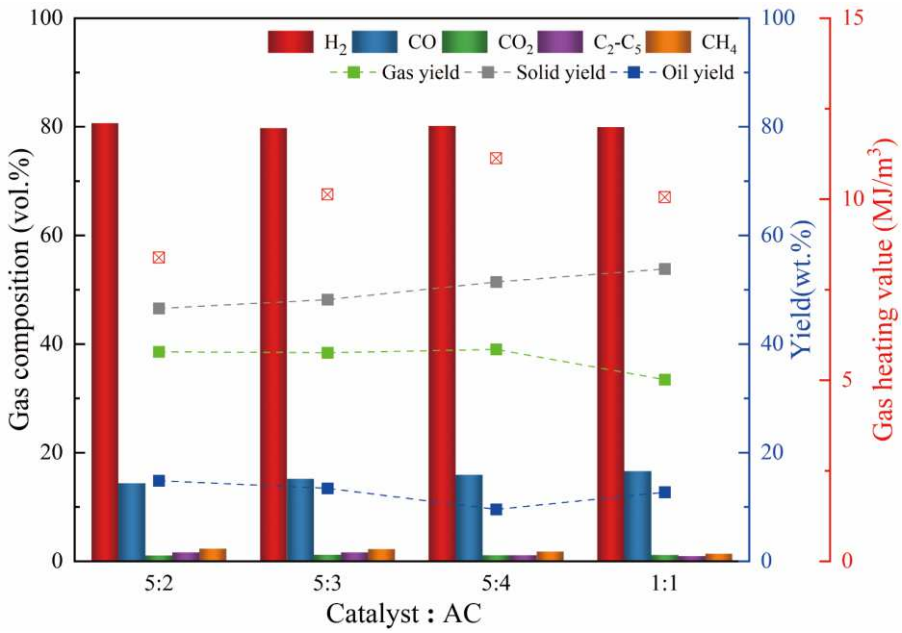


Figure 10 Product distribution and gas composition after microwave pyrolysis of PP at different catalyst-to-absorber mass ratios

3.2.3 Phase Composition Analysis

Figure 11 shows the phase composition of solid products after microwave pyrolysis of PP at different catalyst-to-absorber mass ratios. XRD patterns show that at all mass ratios, the characteristic peaks of $NiFe_2O_4$, γ-Al_2O_3, and PP largely disappeared and were replaced by Fe_3C and $Ni_{0.36}Fe_{0.64}$ solid solution phases, confirming that the catalyst active components were reduced and participated in PP pyrolysis. At 5:2, the Fe_3C and $Ni_{0.36}Fe_{0.64}$ peaks were the weakest, while the Fe_3O_4 peak remained prominent, indicating incomplete reduction of the active components; Fe may still have been present in higher oxidation states. This suggests that the absorber supplied insufficient energy, which limited reduction of the metal active phases and lowered catalytic capacity. At 5:4, the Fe_3C and solid solution peaks reached their highest intensity, the graphite peak was sharp, indicating that pyrolysis favored the formation of highly ordered graphitic carbon. At 1:1, the Fe_3C and solid solution peaks weakened and the disordered carbon peak intensified, as excess activated carbon covered the catalyst active sites and caused local overheating and sintering. This phase evolution is broadly consistent with the trend of H_2 yield first increasing and then decreasing across the mass ratios.

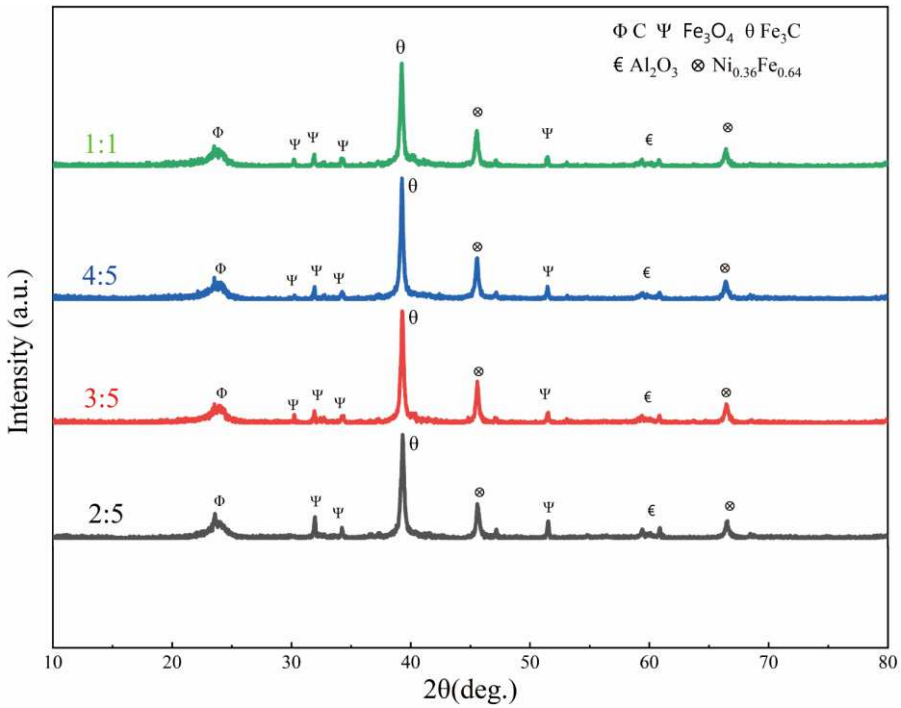


Figure 11 Phase composition after microwave pyrolysis of PP at different catalyst-to-absorber mass ratios

3.2.4 Functional Group Analysis

Figure 12 shows the functional groups and molecular structures of solid products after microwave pyrolysis of PP at different catalyst-to-absorber mass ratios. At all mass ratios, the PP characteristic absorption peaks had disappeared, with only a very weak -CH_3 signal remaining, indicating that the PP macromolecular chains were fully broken down and pyrolyzed. The 5:4 system had the weakest long-chain aliphatic C-C vibration peak, indicating more complete pyrolysis and less residual disordered carbon in the solid product. At lower ratios (5:2, 5:3), the low absorber proportion and insufficient microwave energy conversion led to incomplete PP pyrolysis. At 1:1, excess activated carbon encapsulated the catalyst active sites, which reduced catalyst activity and increased disordered carbon in the solid product. Increasing the activated carbon proportion appropriately supplies more energy to the reaction system, promotes deep dehydrogenation of intermediate macromolecules at the catalyst active sites, and reduces amorphous carbon in the solid residue.

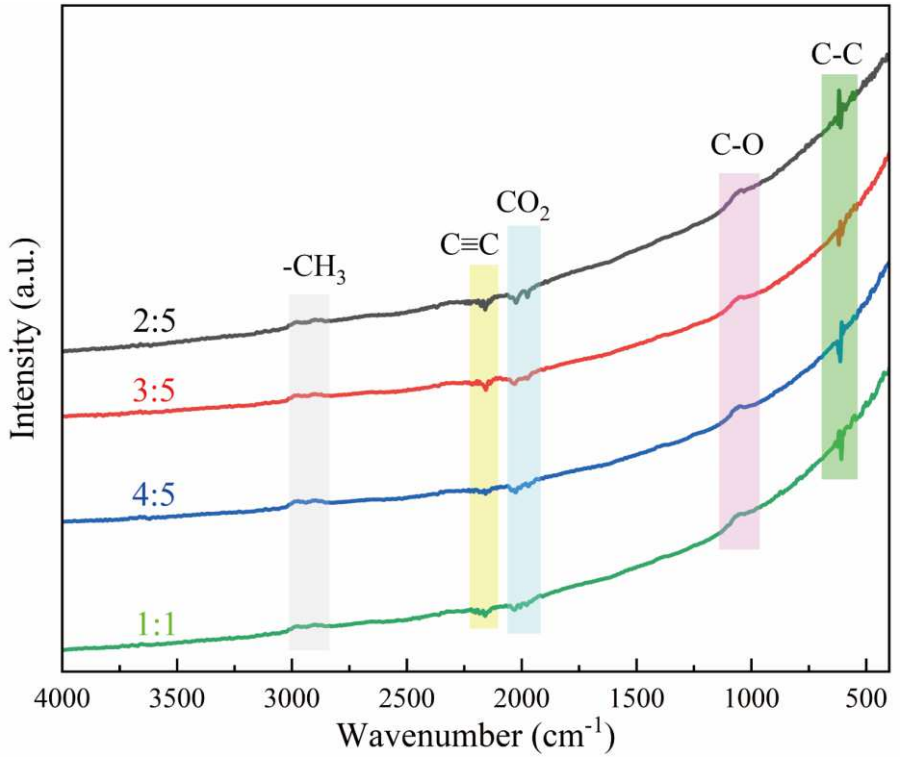


Figure 12 Functional groups and molecular structures of solid products after microwave pyrolysis of PP at different catalyst-to-absorber mass ratios

3.2.5 Morphology Analysis

Figure 13 shows the surface morphology of solid products after microwave pyrolysis of PP at different catalyst-to-absorber mass ratios. At 5:2, the product appeared as large agglomerates, reflecting low absorber proportion, insufficient energy, and incomplete PP pyrolysis. At 5:3, the blocky structure fragmented and some fine particles appeared, indicating more complete pyrolysis. At 5:4, the product had a loose, finely fragmented, and uniformly distributed velvet-like structure. The absorber proportion was optimal here, providing sufficient and uniform heat for the most complete PP pyrolysis. At 1:1, the product showed dense agglomeration and signs of sintering, as excess activated carbon encapsulated active sites and caused local overheating, which hindered PP pyrolysis. These results confirm that the catalyst-to-absorber mass ratio affects pyrolysis efficiency by governing microwave energy conversion and active site exposure.

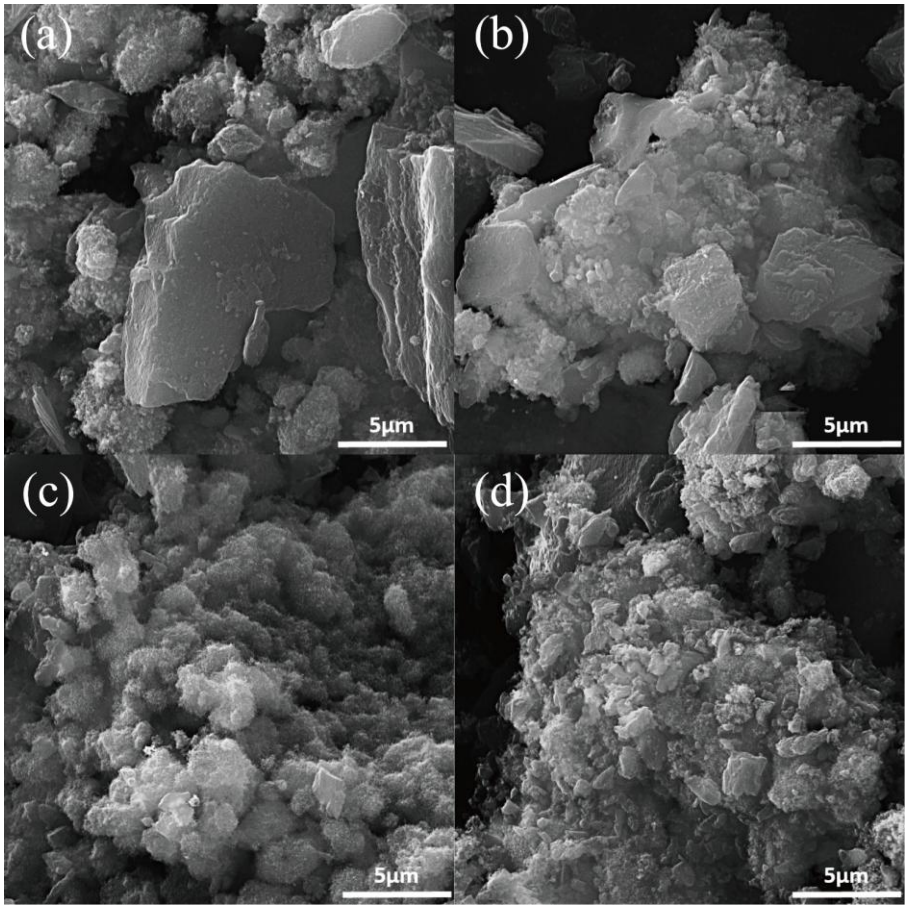


Figure 13 Microstructure of solid products after microwave pyrolysis of PP at different catalyst-to-absorber mass ratios

(a) 5:2; (b) 5:3; (c) 5:4; (d) 1:1

3.3 Effect of Microwave Power on Hydrogen Production Performance

3.3.1 Heating Characteristics

Figure 14 shows the heating curves of microwave pyrolysis of PP at different microwave powers. As power increased from 1200 to 1800 W, the average heating rate after the initial slow stage rose from 24.7 to 118.5 °C/min. At 1200 W, the curve was the most gradual, indicating that at this power the absorber supplied insufficient heat, slowing both bond cleavage in the PP macromolecules and the catalytic reaction. At 1800 W, the heating rate was the fastest: plastic particles volatilized rapidly, and the residence time of pyrolysis intermediates at catalyst active sites was sharply reduced. Some large intermediates escaped into the gas or liquid before deep dehydrogenation was complete, and hydrogen production efficiency decreased. At 1600 W, the heating characteristics balanced sufficient heat supply with reasonable residence time, providing the best temperature conditions for catalytic pyrolysis of PP to hydrogen. Appropriate microwave power thus accelerates the reaction and supplies sufficient energy, promoting extensive cleavage of PP macromolecular chains and the conversion of

macromolecules to small-molecule gases.

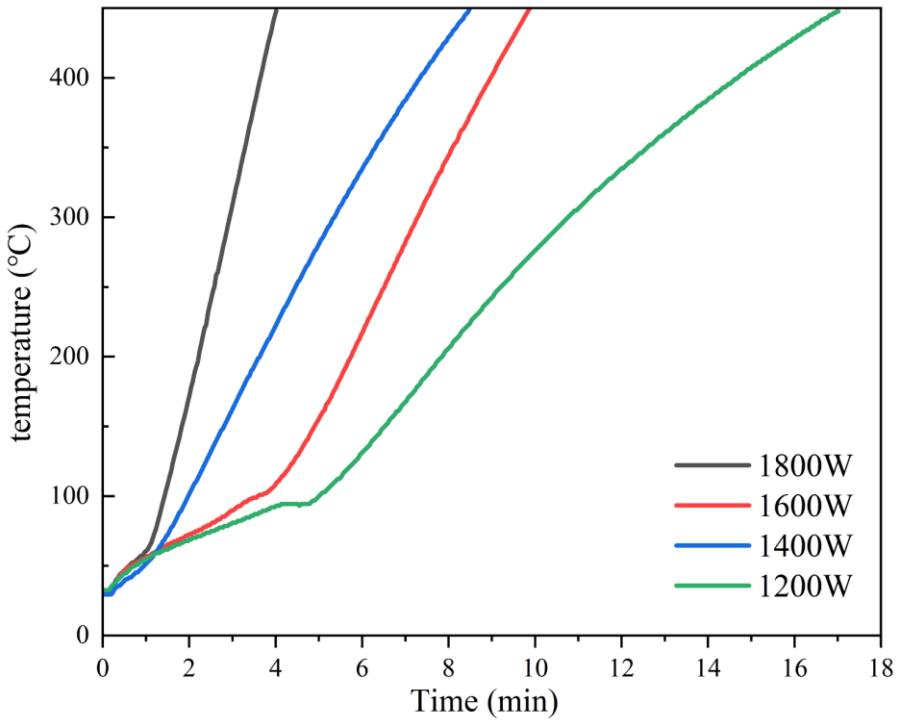


Figure 14 Heating curves of microwave pyrolysis of PP at different microwave powers

3.3.2 Product Distribution and Hydrogen Production Performance

Figure 15 shows the hydrogen production performance of microwave pyrolysis of PP at different microwave powers. As power increased from 1200 to 1600 W, H_2 yield increased from 63.9 to 77.1 mmol/g_{pp} and H_2 efficiency from 73.4% to 88.6%. At 1800 W, H_2 yield decreased to 69.8 mmol/g_{pp}, H_2 efficiency to 80.2%. The 1200, 1400, 1600, and 1800 W systems gave H_2 yields of 63.9, 71.9, 77.1, and 69.8 mmol/g_{pp}, H_2 efficiencies of 73.4%, 82.6%, 88.6%, and 80.2%, respectively. At a catalyst-to-activated-carbon mass ratio of 5:4, the theoretical H_2 yield was 86.1 mmol/g_{pp}. Both H_2 yield and efficiency peaked at 1600 W, the optimal power within the tested range.

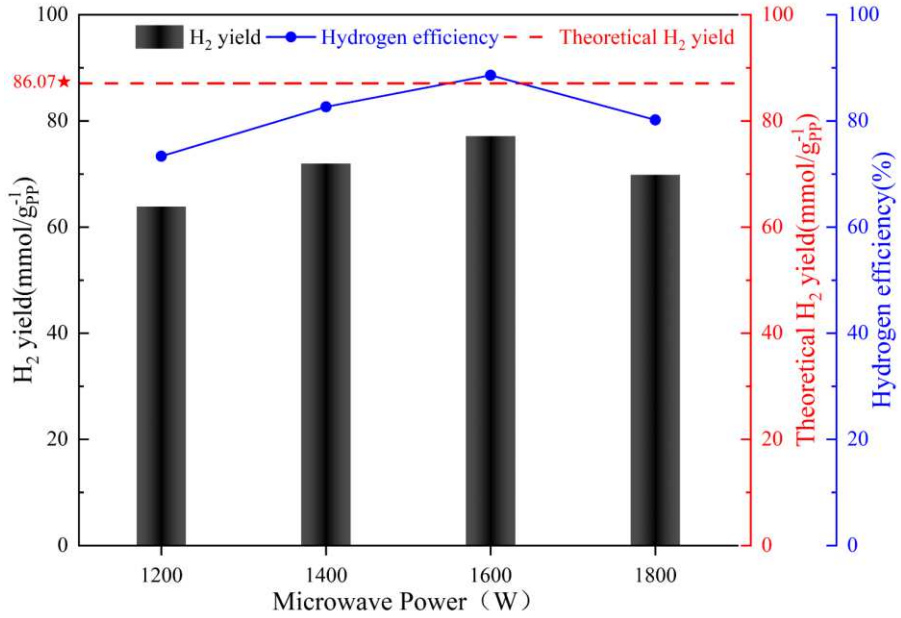


Figure 15 H_2 yield, theoretical yield, and hydrogen production efficiency after microwave pyrolysis of PP at different microwave powers

Figure 16 shows the product distribution and gas composition of microwave pyrolysis of PP at different microwave powers. The 1200, 1400, 1600, and 1800 W systems gave gas yields of 32.9, 34.0, 39.0, and 39.4 wt.%, liquid yields of 14.9, 9.4, 9.5, and 12.4 wt.%, and solid yields of 52.2, 56.6, 51.4, and 48.2 wt.%, respectively. From 1200 to 1600 W, gas yield increased from 32.9 to 39.0 wt.% while liquid yield decreased from 14.9 to 9.5 wt.%. At 1800 W, the gas yield continued to rise to 39.4 wt.%, but the liquid yield rose again from 9.5 to 12.4 wt.%. In the 1600 W system, the gas contained 80.1 vol.% H_2, 15.9 vol.% CO, 1.1 vol.% CO_2, 1.8 vol.% CH_4, and 1.1 vol.% C_2-C_5. At 1800 W, the H_2 composition decreased to 77.6 vol.%, while the CO and CH_4 compositions increased to 17.2 and 2.7 vol.%, respectively, indicating that excessive power caused some macromolecular intermediates to escape as liquid before deep dehydrogenation while also promoting CO formation. The product gas heating value first increased and then decreased with the increase of the microwave powers, peaking at 11.1 MJ/m^3.

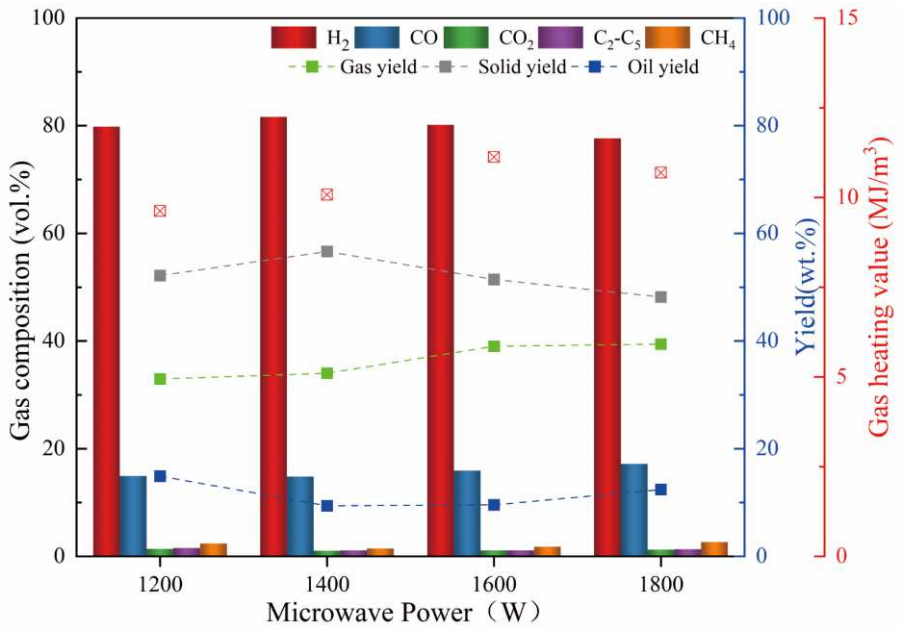


Figure 16 Product distribution and gas composition after microwave pyrolysis of PP at different microwave powers

3.3.3 Phase Composition Analysis

Figure 17 shows the phase composition of solid products after microwave pyrolysis of PP at different microwave powers. XRD patterns show that at all powers, the PP characteristic peaks disappeared, and Fe_3C, $Ni_{0.36}Fe_{0.64}$ solid solution, Fe_3O_4, and graphitic carbon were identified in the products. From 1200 to 1600 W, the diffraction peak intensities of the active phases increased with power, indicating that sufficient microwave energy allowed complete reaction between the catalyst active components and plastic particles. At 1800 W, the Fe_3C and solid solution peaks weakened and the disordered carbon peak broadened, indicating that excessive power caused overly rapid heating and sharply reduced the residence time of volatiles at the active sites. Carbon atoms were deposited as disordered carbon before the Fe_3C intermediate phase could form, and the instantaneous high temperature may also have sintered active sites, leaving deep reforming incomplete. These results confirm that microwave power affects active phase reduction, ordered carbon precipitation, and the degree of catalyst sintering by governing the reaction temperature and heating rate.

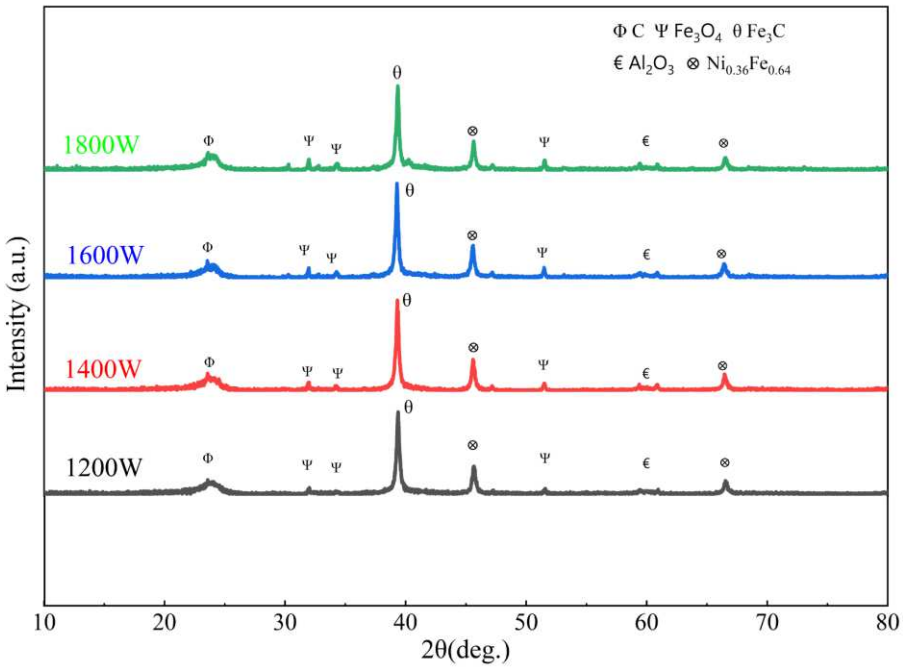


Figure 17 Phase composition after microwave pyrolysis of PP at different microwave powers

3.3.4 Functional Group Analysis

Figure 18 shows the functional groups and molecular structures of solid products after microwave pyrolysis of PP at different microwave powers. At all powers, the PP characteristic absorption peaks had disappeared, with only a very weak absorption peak of -CH_3 remaining, indicating that the PP macromolecular chains were fully broken down and pyrolyzed. At 1600 W, the long-chain aliphatic C-C skeleton peak was the weakest, with less residual disordered carbon, indicating that the moderate heating rate allowed intermediates enough time for deep dehydrogenation. This peak was stronger at both 1200 and 1800 W: at 1200 W because of insufficient heat and suppressed catalyst performance, and at 1800 W because of overly rapid heating and excessively short residence time of intermediate hydrocarbons. In both cases, substantial amounts of incompletely pyrolyzed material remained in the solid product. These results show that microwave power affects the depth of bond cleavage in PP macromolecular chains and the residual carbon skeleton content by governing the heating rate and intermediate reaction time.

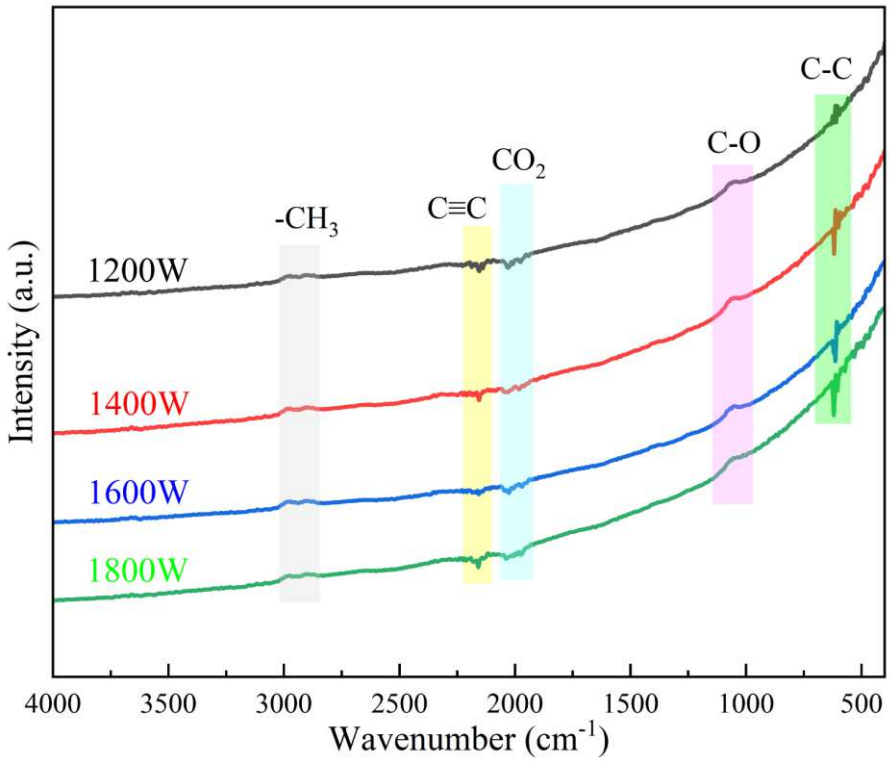


Figure 18 Functional groups and molecular structures of solid products after microwave pyrolysis of PP at different microwave powers

3.3.5 Morphology Analysis

Figure 19 shows the surface morphology of solid products after microwave pyrolysis of PP at different microwave powers. At 1200 W, the product appeared as irregular large blocks with dense surfaces, reflecting insufficient energy, incomplete PP pyrolysis, and coking of macromolecular intermediates on the catalyst surface. At 1400 W, the blocky structure ruptured, with some coarse particles and local adhesion remaining, indicating that pyrolysis was not yet complete. At 1600 W, the product was loose, finely fragmented, and uniformly distributed, as moderate power promoted deep pyrolysis and dehydrogenation of PP. At 1800 W, the product again showed dense agglomeration, as overly rapid heating caused sintering of some active components. These results confirm that microwave power affects pyrolysis depth and catalytic activity by governing the heating rate and volatile residence time.

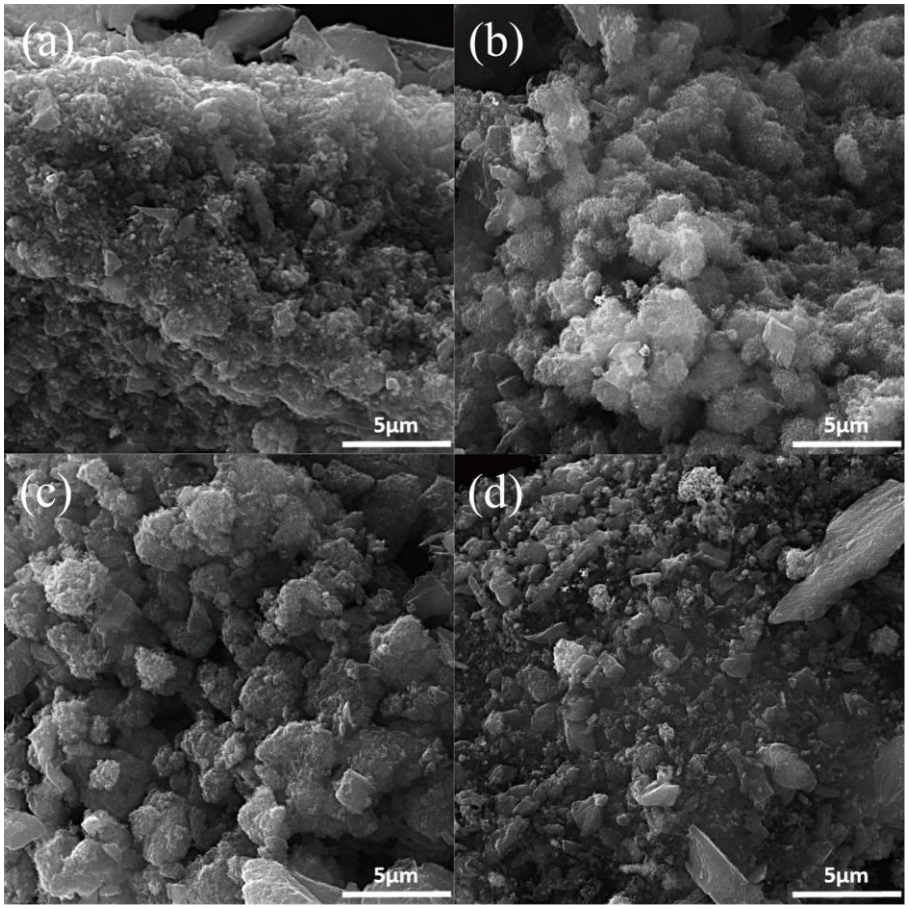


Figure 19 Microstructure of solid products after microwave pyrolysis of PP at different microwave powers

(a) 1200 W; (b) 1400 W; (c) 1600 W; (d) 1800 W

4 Conclusions

This study used PP as the feedstock, Ni-Fe/γ-Al_2O_3 as the catalyst, and activated carbon as the microwave absorber to investigate how absorber type, catalyst-to-absorber mass ratio, and microwave power affect microwave-assisted catalytic pyrolysis for hydrogen production. XRD, SEM, and FT-IR were used to characterize the catalyst before and after the reaction and to examine the synergistic behavior of the absorber-catalyst system in the microwave field. The main conclusions are as follows. At the microwave powers tested, the activated carbon absorber supplied the heat needed for PP pyrolysis. With no absorber added, the material temperature did not reach the threshold for significant pyrolysis, so the reaction hardly proceeded. Coconut-shell activated carbon performed best in microwave absorption and catalytic synergy, owing to its highest specific surface area (1676.14 m^2/g) and well-developed microporous structure. The optimal catalyst-to-absorber mass ratio was 5:4, where microwave energy conversion and the number of catalytic active sites were best balanced; gas yield and H_2 yield peaked at 39.0 wt.% and 77.1 $mmol/g_{pp}$, respectively. It should be noted that part of the hydrogen is attributed to

self-gasification of the activated carbon absorber. Microwave power governed product distribution through the heating rate and volatile residence time; 1600 W balanced sufficient heat supply with reasonable residence time, giving H_2 efficiency of 88.6% and H_2 composition of 80.1 vol.%. In summary, this study preliminarily explored the synergistic characteristics of the activated carbon absorber and the Ni-Fe catalyst in the microwave field, and determined the process window for microwave-assisted catalytic pyrolysis of PP waste plastics for hydrogen production with coconut-shell activated carbon as the absorber. The data also provided experimental evidence and process guidance for the valorization of waste plastics into hydrogen-rich gas.

Acknowledgements

This study was financially supported by the Natural Science Foundation of Inner Mongolia (Grant No. 2025LHMS05017), the Natural Science Foundation of China (Grant No. 52600229), the National Key Research and Development Project (Grant No. 2020YFC1909102), Research Start-up Funds for Public Institutions at the Autonomous Region Level in Inner Mongolia, Basic Research Business Expenses of Inner Mongolia University of Science and Technology, and Research Start-up Fund of Inner Mongolia University of Science and Technology. Thanks to Start-up Funds for Talent Introduction and Scientific Research of Institutions in Inner Mongolia Autonomous Region.

References

[1] Li Y, Liu L, Lee L Q, et al. Electroreforming of plastic wastes for value-added products[J]. Chemical Communications, 2025, 61(1): 33-45.

[2] Vatankhah F, Garcia A C, Chaouki J, et al. Hydrogen and carbon nanotube production from microwave-assisted catalytic decomposition of plastic waste[J]. Chemical Engineering Journal, 2025, 503: 158189.

[3] Niu F, Wu Z, Chen D, et al. State-of-the-art and perspectives of hydrogen generation from waste plastics[J]. Chemical Society Reviews, 2025, 54(10): 4948-4972.

[4] Cao Y, Xiang H J, Yan Y, et al. Catalyst design for microwave-enhanced hydrogen production: Comparative performance across diverse feedstocks[J]. Catalysis Today, 2026, 461: 115523.

[5] Dan E, McCue A J, Dionisi D, et al. Plastic valorization into added-value products via microwave and conventional pyrolysis: A review[J]. ACS Environmental Au, 2026, 6(2): 174.

[6] Irfan M, Saleem R, Shoukat B, et al. Production of combustible fuels and carbon

nanotubes from plastic wastes using an in-situ catalytic microwave pyrolysis process. [J]. Scientific Reports, 2023, 13: 9057.

[7] Calero M, Solís R R, Muñoz-Batista M J, et al. Oil and gas production from the pyrolytic transformation of recycled plastic waste: An integral study by polymer families[J]. Chemical Engineering Science, 2023, 271: 118569.

[8] Abbas-Abadi M S, Ureel Y, Eschenbacher A, et al. Challenges and opportunities of light olefin production via thermal and catalytic pyrolysis of end-of-life polyolefins: Towards full recyclability[J]. Progress in Energy and Combustion Science, 2023, 96: 101046.

[9] Suriapparao V. D, Garlapati N, Attada Y, et al. Optimization of microwave power and graphite susceptor quantity for waste polypropylene microwave pyrolysis[J]. Process Safety and Environmental Protection, 2021, 149: 234-243.

[10] Peng Y, Wang Y, Ke L, et al. A review on catalytic pyrolysis of plastic wastes to high-value products[J]. Energy Conversion and Management, 2022, 254: 115243.

[11] Yao D, Zhang Y, Williams P T, et al. Co-production of hydrogen and carbon nanotubes from real-world waste plastics: Influence of catalyst composition and operational parameters[J]. Applied Catalysis B: Environmental, 2018, 221: 584-97.

[12] Luo J, Gong G, Ma R, et al. Study on high-value products of waste plastics from microwave catalytic pyrolysis: Construction and performance evaluation of advanced microwave absorption-catalytic bifunctional catalysts[J]. Fuel, 2023, 346: 128296.

[13] Deng J, Meng L, Ma D, et al. High H_2 selective performance of Ni-Fe-Ca/H-Al catalysts for steam reforming of biomass and plastic[J]. Journal of Energy Chemistry, 2023, 80: 215-227.

[14] Liu C, Qin J, Zhu Z, et al. Energy-saving microwave-assisted catalysis over SiC@NiFe for selective valorization of plastic wastes into H_2 and carbon nanotubes[J]. Small, 2026, 22(3): e08065.

[15] Cai N, Xia S W, Li X Q, et al. High-value products from ex-situ catalytic pyrolysis of polypropylene waste using iron-based catalysts[J]. Waste Management, 2021, 136: 47-56.

[16] Song Z, Yao L, Jing C, et al. Drying behavior of lignite under microwave heating [J]. Drying Technology, 2017, 35(4): 433-443.

[17] Marchetti L, Doszczeczko S, Tognotti L, et al. Auto-catalytic effect of iron on plastic solid waste pyrolysis[J]. ACS Sustainable Chemistry & Engineering, 2026, 14(29): 13303-13315.

[18] Rodriguez-Gomez A, Ould-Chikh S, Castells-Gil J, et al. Fe-MOF materials as precursors for the catalytic dehydrogenation of isobutane[J]. ACS Catalysis, 2022, 12(7): 3832-3844.